Imaging system of a plasma torch of a Betatron X-ray source

© E.S. Antyushin,[1] A.A. Akhsakhalyan,[1] S.Yu. Zuev,[1] A.Ya. Lopatin,[1] I.V. Malyshev,[1] A.N. Nechay,[1] A.A. Perekalov,[1] A.E. Pestov,[1] N.N. Salashchenko,[1] M.N. Toropov,[1] B.A. Ulasevich,[1] N.N. Tsybin,[1] N.I. Chkhalo,[1] A.A. Soloviev,[2] M.V. Starodubtsev[2]

[1] Institute of Physics of Microstructures, Russian Academy of Sciences,
607680 Nizhny Novgorod, Russia
[2] Institute of Applied Physics, Russian Academy of Sciences,
603950 Nizhny Novgorod, Russia
e-mail: aepestov@ipm.sci-nnov.ru

The paper describes the design of a microscope for studying a betatron radiation source based on the PEARL femtosecond laser complex in the SXR and EUV wavelength range. The main optical element of the microscope is a spherical Schwarzschild objective a x5 magnification. The device allows to study the size and spatial structure of the interaction area of laser radiation with matter, at a selected wavelength in the EUV or SXR range with a resolution of $\delta x = 2.75\,\mu$m. The operation wavelength ($\lambda = 13.5$ nm) is set by multilayer X-ray mirrors. Thin-film absorption filters are used to suppress the background component of the signal.

Keywords: SXR and EUV radiation, betatron radiation, imaging x-ray optics, SXR microscope.

Introduction

Considerable interest in extreme light fields, which in the future can provide information about the space-time structure and nonlinear optical properties of vacuum, and the physics of their effect on matter, forces researchers to study the mechanisms of interaction of super-powerful laser pulses with various targets (gas jets, gas clusters, solid). When an extreme intensity laser pulse interacts with a substance, X-ray radiation is generated. The simplest generation mechanism is the braking mechanism, since the electron energy is sufficient to emit optical quanta up to the X-ray wavelength range. The braking mechanism implies a wide, decreasing with increasing quantum energy, radiation spectrum without any pronounced features. However, the interaction region can be a source of not only braking, but also characteristic radiation. The characteristic radiation has pronounced spectral peaks, the type of which is determined by the composition, concentration and temperature of the resulting plasma. Moreover, the shells of atoms can be excited both due to collisions with electrons and due to the absorption of high-energy braking quanta [1]. At the same time, there are also more efficient laser-plasma mechanisms for generating short-wave radiation, mainly associated with the collective movement of charged particles caused by an acutely focused laser pulse. X-ray generation from a betatron source is associated with collective mechanisms [2–5]. Betatron radiation — is the radiation of charged particles during oscillation in an electromagnetic field. In this case, laser-induced electron acceleration (Laser WakeField Acceleration — LIFE) occurs when laser pulses of femto- and nanosecond duration interact with a laser target. The nature of this effect is as follows. When interacting with powerful pulses of short duration, plasma ionization occurs already at the leading edge of the laser beam, and its main part excites a wake wave in the gas, the wake wave electrons oscillate in the field of the electromagnetic laser wave, resulting in radiation generation. The spectral characteristics of such sources are devoid of resonant features inherent in characteristic spectra. However, due to the resonant nature of the interaction with the laser pulse, such sources can be very localized. Indirect estimates of the geometric dimensions of the betatron source demonstrated in the experiment [6] showed that its size does not exceed 2 mm. The radiation of a betatron source has a fairly wide spectrum from eV units to tens of keV (depending on the parameters of the laser pulse and the concentration profile of the transparent plasma) [7]. On the other hand, it is known that the corresponding structure of the electron beam at the exit from the interaction region can be quite complex. For example, in the study [8] it is shown that, depending on the P/Pcr ratio (the ratio of the laser pulse power to the critical power for relativistic self-focusing), electron beams can be either single or „clustered". In this regard, direct visualization of the source is of great interest, which will provide information about its spatial structure and will allow you to gain new knowledge about the physics of the interaction of powerful laser radiation with matter. Such studies are planned to be carried out on the basis of the PEARL femtosecond laser complex (IAP RAS) [9].

Since the generation occurs in the X-ray wavelength range, the main methods for diagnosing processes occurring as a result of the interaction of laser radiation with matter are X-ray. However, the task of experimental investigation
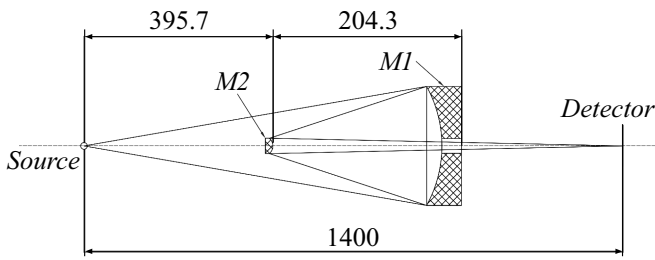
Figure 1. X-ray optical scheme of the microscope. *M1* — primary concave mirror Ø7.2 mm; *M2* —secondary convex mirror Ø12.0 mm.
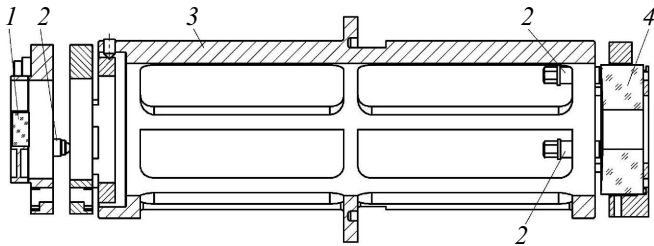
Figure 2. Lens design: *1* — convex mirror *M2*; *2* — adjustment screws; *3* — lens housing; *4* — concave mirror *M2*.

of the laser spark region is quite difficult. To solve it, it is necessary to use high-resolution imaging systems based on multilayer X-ray mirrors (MLM). This paper describes the design and principles of operation of a specially designed microscope that allows measuring the geometric dimensions and investigating the structure of a laser spark with a micron spatial resolution.

1. Microscope design

The device is built according to the scheme of a Schwarzschild lens with two spherical mirrors and a magnification of x5. The calculation of the optical scheme of the microscope was carried out in the Zemax [10] software

package. The calculated geometric parameters of the device are shown in Fig. 1.

As a recording element in the device, a CCD matrix Andor DX440-BN, with a pixel size of $13.5 \times 13.5 \mu$m, matrix area of 27.6×6.9 mm is used[2] (2048×512 pixels). The calculated „pixel" resolution (the radiation source in the plane of an object up to $2.75 \times 2.75 \mu$m will focus in 1 the pixel of the matrix with the size of $13.5 \times 13.5 \mu$m) of the device is achieved with aberration distortion of the wavefront by the parameter RMS is no more than 4.5 nm and is 2.75μm in the plane of the object with a field of view of 1.2×1.2 mm.

The physical dimensional parameters of the substrates for MLM were: *M 1* (concave) outer diameter — 46 mm, inner — 14 mm, radius of curvature — 27.0 mm; *M2* (convex) diameter — 12 mm, radius of curvature — 405.5 mm. The design of the lens is shown in Fig. 2.

To ensure the coaxial installation of mirrors, a solid-chiseled housing design was chosen. The mounting of the MLM frames was carried out with the help of clamping screws. To accurately set the distance between the mirrors for a concave mirror (*M1*), adjustment is provided using adjusting screws. The detector is connected to the vacuum volume of the microscope through a specialized flange, which simplifies the preliminary adjustment of the device.

2. Correction of wavefront aberrations

To ensure „pixel" resolution, the correction of wave aberrations introduced by the lens was carried out, since the surfaces made by mechanical lapping after assembly showed wavefront errors at the RMS ~ 13 nm level. Wavefront errors were corrected by correcting the shape of the „large" concave mirror *M1* by ion beam etching. The technique of correcting local shape errors by small-sized and wide-aperture ion beams is described in detail in [11]. After three iterations (one axisymmetric by a wide-aperture ion beam and two local by a small-sized ion beam), the wavefront errors of the primary mirror *M1* were reduced by more
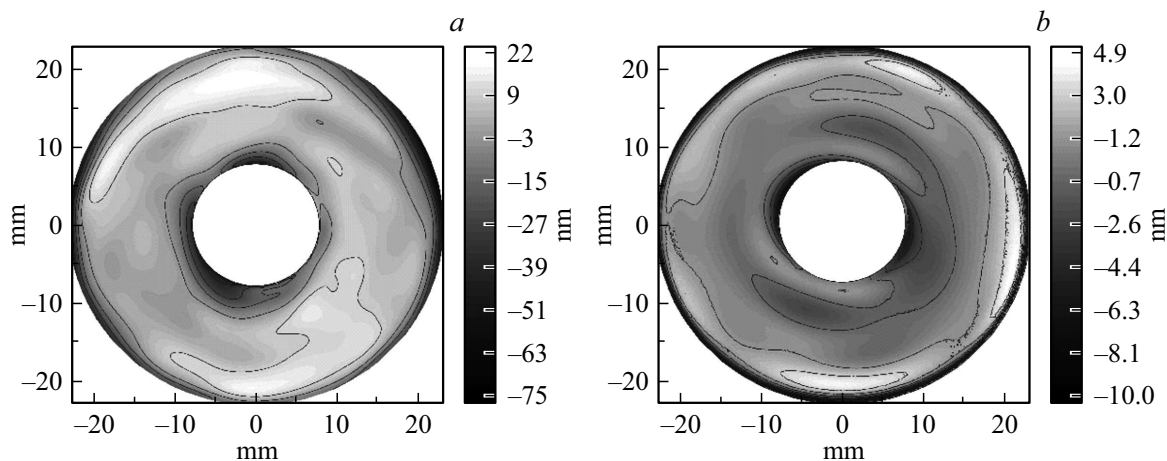
Figure 3. Mirror surface map *M1*: *a* — before ionic correction (RMS = 12.8 nm); *b* — after ionic correction (RMS = 2.1 nm).
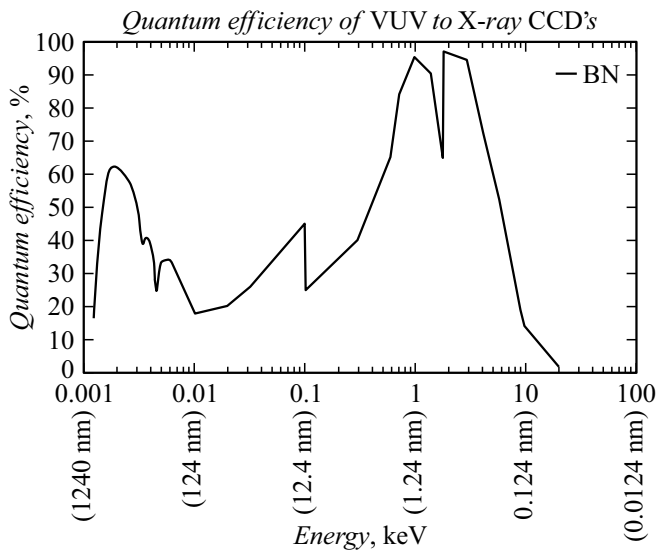
Figure 4. Spectral sensitivity of the Andor DX440-BN X-ray 2D detector.
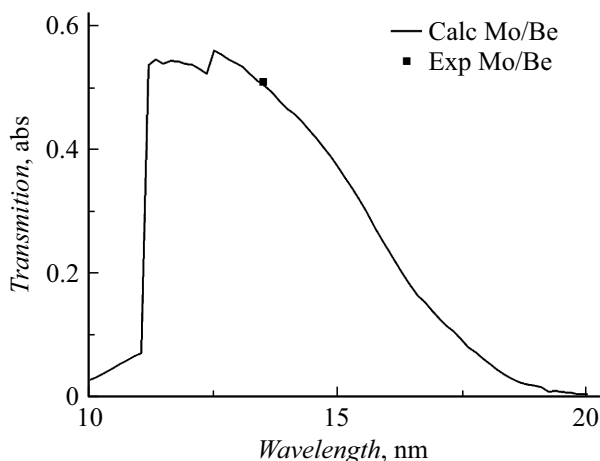
Figure 5. The transmission coefficient of the Mo/Be filter, calculation (solid) experiment (point).
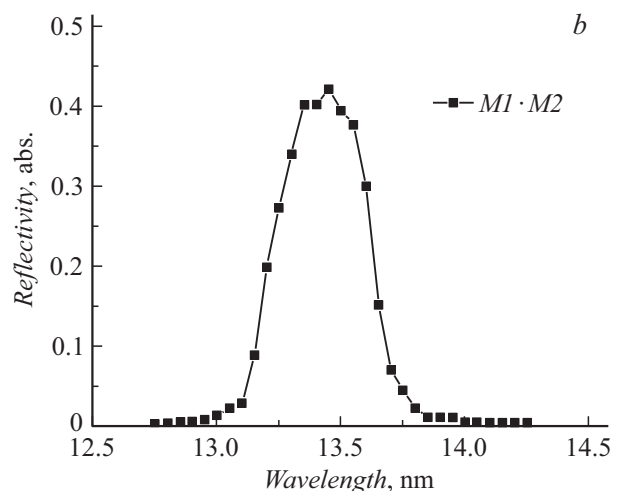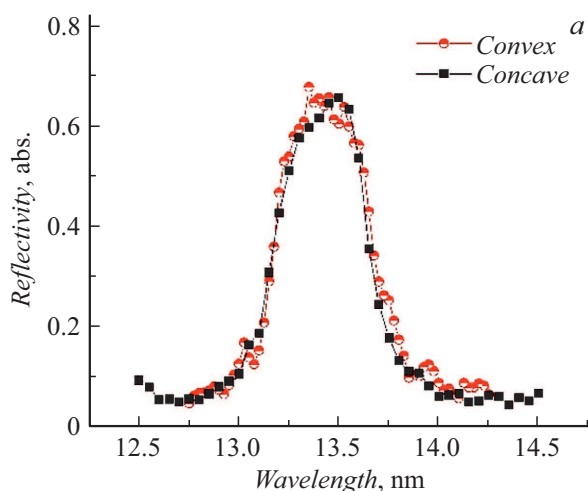
than 6 times to RMS ~ 2.1 nm. Maps of the surface shape error $M\ 1$ before and after correction are shown in Fig. 3.

3. X-ray optical elements

As the working wavelength of the device, $\lambda = 13.4$ nm was chosen (the working wavelength of the projection EUV lithography). All X-ray optical elements were optimized for this wavelength.

The spectral sensitivity of the detector [12] is shown in Fig. 4.

To suppress the long-wave background (visible and UV radiation), a thin-film absorption filter is installed at the input of the device and directly in front of the SXR and EUV radiation detector. In this case, a structure based on a pair of molybdenum and beryllium materials was developed. The structure began and ended with a thin film of molybdenum silicide ($MoSi_2$), the so-called cap layer, which protects molybdenum from oxidation and, as a consequence, degradation of X-ray optical properties. Thus, the filter structure was as follows: $MoSi_2(2.5$ nm$)/Mo(2$ nm$)/(Be-3$ nm, $Mo-2$ nm$)*30$ periods$/MoSi_2(2.5$ nm$)$. The total thickness of the filter was 157 nm. The calculated spectral dependence of the filter transmittance and measured at the operating wavelength ($\lambda = 13.4$ nm) are shown in Fig. 5.

Multilayer Mo/Si X-ray mirrors optimized for a wavelength of 13.4 nm were applied to substrates with a corrected surface shape as reflective coatings. In order to preserve the quality of the shape of the surfaces and, as a consequence, the spatial resolution of the device, the technology of compensation of internal stresses in films was applied. The technique of compensation of internal stresses in structures based on a pair of Mo and Si materials is described in detail in [14]. The reflective characteristics of the lens mirrors obtained on the [15] reflectometer are shown in Fig. 6.

Figure 6. Spectral dependences of the reflection coefficient of the lens mirrors (a) and their convolution (b).
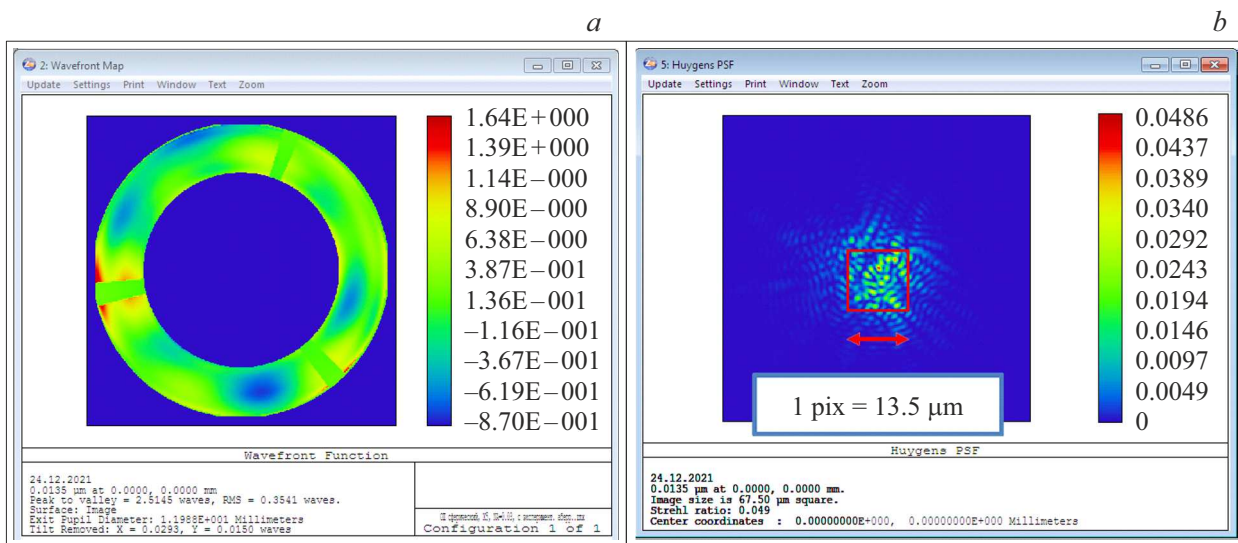
Figure 7. Lens aberration map $(RMS = 4.5\,nm)$ (a) and focus spot (b). Calculation in the Zemax program.

After assembling the lens on an interferometer with a diffraction wave of comparison [16], the wave aberrations of the device were measured. Fig. 7, a shows a map of the aberrations of the Schwarzschild lens obtained after assembling the device.

As you can see, the wave aberrations of the device after applying multilayer X-ray mirrors to the surface of the substrates and assembling the lens amounted to RMS=4.5 nm, which provides „pixel" resolution. The calculated focusing spots for this wave aberration map obtained in the Zemax software are shown in Fig. 7, b.

Conclusion

An X-ray microscope with a magnification of x5 and a field of view of $1.2 \times 1.2\,mm$ based on a two-mirror spherical Schwarzschild lens has been developed. The correction of the mirror substrates was carried out, which made it possible to obtain wave aberrations according to the RMS = 4.5 nm parameter and provide „pixel" resolution of the device when using the Andor DX440-BN CCD sensor as a detector, with a pixel size of $13.5 \times 13.5\,\mu m$, matrix area $27.6 \times 6.9\,mm^2$ $(2048 \times 512\,pixels)$. The calculated spatial resolution of the microscope in the sample plane was $\delta x = 2.75\,\mu m$.

The multilayer X-ray mirrors optimized for the working wavelength of modern EUV nanolithography ($\lambda = 13.4\,nm$) provided high (more than 40%) transmission of the optical system, which in combination with highly transparent (more than 50%) in the vicinity of the wavelength of 13.4 nm free-hanging absorption filters will allow have a high time resolution of the device, which will allow recording the signal in one laser pulse.

Conflict of interest

The authors declare that they have no conflict of interest.

References

[1] A.Ya. Faenov, J. Colgan, S.B. Hansen, A. Zhidkov, T.A. Pikuz, M. Nishiuchi, S.A. Pikuz, I.Yu. Skobelev, J. Abdallah, H. Sakaki, A. Sagisaka, A.S. Pirozhkov, K. Ogura, Y. Fukuda, M. Kanasaki, N. Hasegawa, M. Nishikino, M. Kando, Y. Watanabe, T. Kawachi, S. Masuda, T. Hosokai, R. Kodama, K. Kondo. Scientific Reports, **5**, 13436 (2015).

[2] I. Kostyukov, A. Pukhov, S. Kiselev. Phys. Plasmas, **11**, 5256 (2004).

[3] W. Lu, C. Huang, M. Zhou, W. Mori, T. Katsouleas. Phys. Rev. Lett., **96**, 165002 (2006).

[4] S. Kiselev, A. Pukhov, I. Kostyukov. Phys. Rev. Lett., **93**, 135004 (2004).

[5] S. Corde, K.Ta Phuoc, G. Lambert, R. Fitour, V. Malka, A. Rousse, A. Beck, E. Lefebvre. Rev. Mod. Phys., **85**, 1 (2013).

[6] J. Wenz, S. Schleede, K. Khrennikov, M. Bech, P. Thibault, M. Heigoldt, F. Pfeiffer, S. Karsch. Nature Commun., **6**, 7568 (2015).

[7] Zs. Lecz, A. Andreev, N. Hafz. Phys. Rev. E, **102**, 053205 (2020). https://doi.org/10.1103/PhysRevE.102.053205

[8] A.A. Soloviev et al. NIM A, **653**, 35–41 (2011).

[9] V.V. Lozhkarev G.I. Freidman, V.N. Ginzburg, E.V. Katin, E.A. Khazanov, A.V. Kirsanov, G.A. Luchinin, A.N. Mal'shakov, M.A. Martyanov, O.V. Palashov, A.K. Poteomkin, A.M. Sergeev, A.A. Shaykin, I.V. Yakovlev. Laser Phys. Lett., **4**, 421 (2007).

[10] [Electronic resource] Available at: www.zemax.com

[11] I.G. Zabrodin, M.V. Zorina, I.A. Kas'kov, I.V. Malyshev, M.S. Mikhailenko, A.E. Pestov, N.N. Salashchenko, A.K. Chernyshev, N.I. Chkhalo. Tech. Phys., **65** (11), 1837–1845 (2020). DOI: 10.1134/S1063784220110274

[12] [Electronic source] Available at: https://andor.oxinst.com/

[13] [Electronic source] Available at: http://xray-optics.ru/products/software-multifitting/

[14] S.S. Andreev, N.N. Salashchenko, L.A. Suslov, A.N. Yablonsky, S.Yu. Zuev. NIM A, **470** (1−2), 162–167 (2001).

[15] S.A. Garakhin, N.I. Chkhalo, I.A. Kas'kov, A.Ya. Lopatin, I.V. Malyshev, A.N. Nechay, A.E. Pestov, V.N. Polkovnikov, N.N. Salashchenko, M.V. Svechnikov, N.N. Tsybin, I.G. Zabrodin, S.Yu. Zuev. Rev. Sci. Instrum., **91** (6), 063103 (2020). DOI: 10.1063/1.5144489

[16] N.I. Chkhalo, I.V. Malyshev, A.E. Pestov, V.N. Polkovnikov, N.N. Salashchenko, M.N. Toropov, A.A. Soloviev. Appl. Opt., **55** (3), 619–625 (2016).